ACS APPLIED MATERIALS & INTERFACES

Research Article

www.acsami.org

Persistent Luminescent Nanocarrier as an Accurate Tracker in Vivo for Near Infrared-Remote Selectively Triggered Photothermal Therapy

Bin Zheng,[†,#] Hong-bin Chen,[†,#] Pei-qi Zhao,[‡] Hui-zhuo Pan,[†] Xiao-li Wu,[†] Xiao-qun Gong,[†] Han-jie Wang,[*,†] and Jin Chang[*,†]

[†]School of Life Sciences, Tianjin University, Tianjin Engineering Center for Micro-Nano Biomaterials and Detection-Treatment Technology, 92 Weijin Road, Nankai District, Tianjin 300072, P.R. China

[‡]Department of Lymphoma, Tianjin Medical University Cancer Institute and Hospital, National Clinical Research Center of Cancer, Sino-US Center for Lymphoma and Leukemia, Key Laboratory of Cancer Prevention and Therapy, Tianjin 300060, China

Supporting Information

ABSTRACT: Optical imaging-guidance of indocyanine green (ICG) for photothermal therapy (PTT) has great latent capacity in cancer therapy. However, the conventional optical image-guidance mode has caused strong tissue autofluorescence of the living tissue, which leads to the accurate infrared light irradiation cannot be conducted. In this article, ICG and persistent luminescence phosphors (PLPs) coloaded mesoporous silica nanocarriers ((ICG+PLPs)@$mSiO_2$) were first designed and prepared for persistent luminescent imaging-guided PTT. The (ICG+PLPs)@$mSiO_2$ nanocarriers could significantly improve signal-to-noise ratio during luminescence imaging-guided PTT, making the PLP promising for improving the accuracy of the tumor site for photothermal therapy in vivo. This paper is likely to develop a new way for accurately regulating cancer cell death based on luminescence imaging-guided PTT selectively triggered by near-infrared (NIR)-remote.

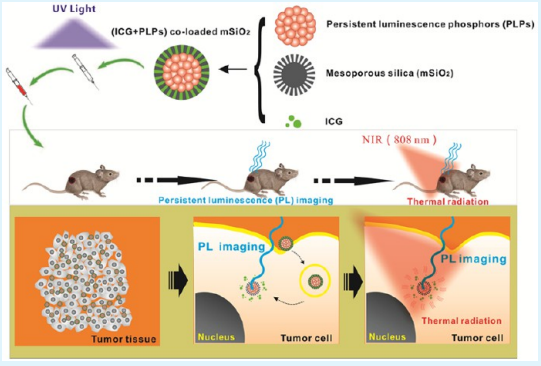

KEYWORDS: *indocyanine green (ICG), near-infrared light (NIR), photothermal therapy (PTT), luminescent nanoprobes, persistent luminescence phosphors (PLPs)*

INTRODUCTION

Near-infrared (NIR, 700−1000 nm) light initiated photothermal therapy (PTT) agents, such as gold nanoparticles and CuS nanoparticles,[1−3] with the deep tissue penetrability and minimally invasive for the organism have attracted much interest in tumor therapy.[4−6] Among the NIR photothermal therapy agents, indocyanine green (ICG), the only water-soluble one that is approved by FDA, works as an anionic tricarbocyanine dye. The ICG can strongly absorb around 808 nm near-infrared light with minimal scattering and fluorescence interference by biomolecules.[7−9] To further enhance the fluorescence stability of ICG in vivo, various nanocarriers, polymer and silica nanoparticles, for example, have been developed to encapsulate ICG.[10−12] So the ICG loaded nanoparticles as new generation photothermal therapy agents could be widely utilized clinically for photothermal therapy.

However, on the basis of the weak fluorescence signal, the conventional ICG loaded nanoparticles cannot be tracked after injected into body, so it is impossible to conduct the accurate irradiation by the extra near-infrared light (NIR, 700−1000 nm) laser.[13−15] Fortunately, optical imaging-guided therapy has attracted more and more interest in recent years, which may be a good choice for tracking the ICG loaded nanoparticles for PTT. It has wide application prospect for fine distinguishability on biological tissues parameters, which can be used for tracking the ICG loaded nanoparticles in vivo for inducing tumor cell death by NIR-remote selective irradiation.

Nowadays, a variety of nanofluorescence probes,[16−18] quantum dots (QDs), and dye-loaded nanocarriers, for instance, have been widely used in optical imaging. Normally these luminescent nanoprobes are excited by visible light below 650 nm, but such light can be significantly absorbed by living tissues, leading to strong tissue autofluorescence.[19,20] The near-infrared fluorescent nanoprobes such as CuS QDs have been reported for decreasing the background noise during imaging; however, the stimulation in vitro is still needed during imaging and the wavelength is still below 650 nm. So the optical image-guided ICG is still hampered by the autofluorescence of the living tissues.

To significantly reduce the strong tissue autofluorescence during luminescent imaging, several methods have been developed. Among these methods, "persistent luminescence

Received: June 23, 2016
Accepted: August 5, 2016
Published: August 5, 2016

DOI: 10.1021/acsami.6b07642
ACS Appl. Mater. Interfaces 2016, 8, 21603−21611

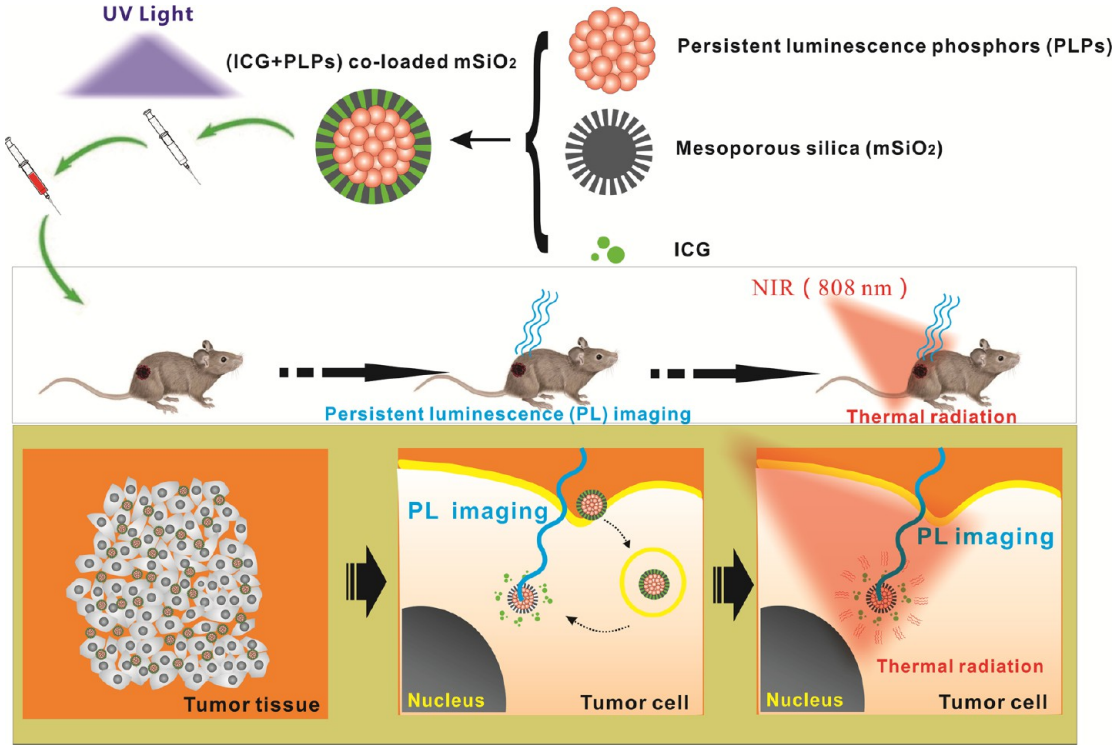

Figure 1. Schematic diagram showed the applications of nanoparticles for persistent luminescent imaging-guided PTT in vivo. In this schematic illustration, the ICG and persistent luminescence phosphors coloaded mesoporous silica nanoparticles consisted of three parts: (1) The persistent luminescent phosphors were chosen as persistent luminescent phosphors, which could be excited by extra light and emit a persistent luminescence for tracking the nanoparticles in vivo. (2) Indocyanine green (ICG), which absorbed near-infrared light and converted effectively into photothermal response, had been used for PTT treatment. (3) The mesoporous silica nanosphere played a role as a three dimensional hard template for stowing and protecting the PLPs and ICG effectively from aggregation and diffusion in vivo. The (ICG+PLPs)@$mSiO_2$ nanoparticles were injected into the tumor of living mouse after ultraviolet light irradiation. The tumor region was irradiated by 808 nm NIR light, according to the persistent luminescent imaging results. The ICG within (ICG+PLPs)@$mSiO_2$ nanoparticles fleetly produce heat after absorbing 808 nm NIR light to implement the kill of a mass of tumor cells.

phosphors" have been paid more and more attention to recently.[21−23] Persistent luminescence phosphors (PLPs) can reserve the excitation energy and then slowly release it by emitting a particular wavelength of photons. The long lasting phosphorescence can sustain for a few hours after removing the excitation light source, which offers much convenience in vivo bioluminescence imaging.[24−26] Compared with conventional fluorescent nanoprobes, PLPs have high signal-to-noise ratio by averting biological tissue autofluorescence caused by persistent excitation in situ of the organism.[27,28]

In this paper, the ICG and persistent luminescence phosphors coloaded mesoporous silica nanoparticles ((ICG +PLPs)@$mSiO_2$) have been developed for persistent luminescent imaging-guided PTT. This new kind of (ICG+PLPs)@$mSiO_2$ nanoparticles could improve the signal-to-noise ratio during luminescence imaging-guided PTT. The (ICG+PLPs)@$mSiO_2$ nanoparticle consists of three parts: (1) The $CaZnTiO_3$:0.1% Pr^{3+} persistent luminescent phosphors were chosen as persistent luminescent phosphors, which could be excited by extra light and emit a persistent luminescence for tracking the nanoparticles in vivo; (2) ICG, with a large number of absorbed near-infrared wavelength region light and effective photothermal response, had been used for PTT treatment; (3) The mesoporous silica nanosphere played a role as a three dimensional hard template for stowing and protecting the PLPs and ICG effectively from aggregation and diffusion in vivo. This new photothermal therapy agent could be used as a novel technique to precisely kill the cancer cell by persistent luminescence phosphors imaging-guided PTT in vivo (as shown in Figure 1).

RESULTS AND DISCUSSION

Characterization of the (ICG+PLPs)@$mSiO_2$ Nanoparticles. The formation process of the (ICG+PLPs)@$mSiO_2$ nanoparticles was shown in Figure 2A. The complete assembly process could be split into three steps. First, the persistent luminescence phosphor (PLPs) clusters were synthesized by the sol−gel method at 1100 °C. For enhancing stability and hydrophilic property, hydrophobic PLPs were coated by a mesoporous silica layer by the cetyltrimethylammonium bromide (CTAB) template method. Finally, the indocyanine green (ICG) as the photothermal therapy agent was loaded into the mesopores of PLPs@$mSiO_2$. Such ICG and PLPs coloaded mesoporous silica nanoparticles ((ICG+PLPs) @$mSiO_2$) were integrated into the special optical property of the red long afterglow with PTT effectively.

Physicochemical characteristics of as-obtained products were tested by X-ray diffraction (XRD), transmission electron microscopy (TEM), and energy-dispersive X-ray spectroscopy (EDX). The XRD was used for confirming crystal structures of the PLPs. These data (Figure 2B) showed that there were relevant diffraction characteristics (peaks at 20°, 30°, 35°, 50°, 60°) of the PLPs, which were consistent with the existing phase of PLP.[29] Detailed morphological features of PLPs@$mSiO_2$ and

DOI: 10.1021/acsami.6b07642
ACS Appl. Mater. Interfaces 2016, 8, 21603−21611

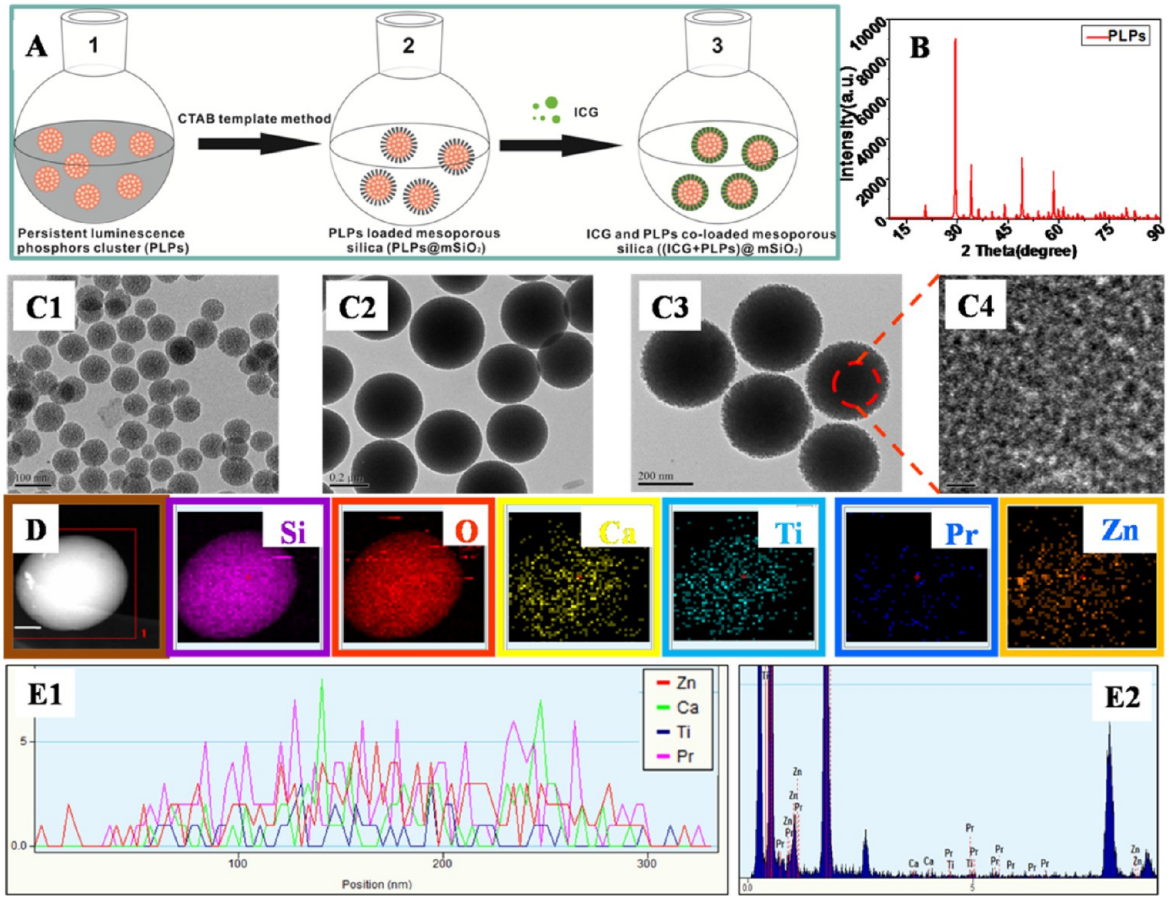

Figure 2. (A) Schematic diagram of manufacture of the (ICG+PLPs)@$mSiO_2$ nanoparticles; (B) XRD data of PLPs nanoparticles. The TEM images of (C1) $mSiO_2$ nanoparticles, (C2) PLPs@$mSiO_2$ nanoparticles, and (C3, C4) (ICG+PLPs)@$mSiO_2$ nanoparticles. (D, E1) The EELS line scan conducted with STEM imaging for element analysis of (ICG+PLPs)@$mSiO_2$ nanoparticle. (E2) The EDX test for element analysis of (ICG+PLPs)@$mSiO_2$ nanoparticle.

(ICG+PLPs)@$mSiO_2$ were examined by TEM. In Figure 2C, the PLPs cluster was encapsulated into the silica shell successfully. The particle sizes and morphologies of the PLPs@$mSiO_2$ nanoparticles and (ICG+PLPs)@$mSiO_2$ nanoparticles showed no significant differences. Both of them had good monodispersity and much clear profile, and their average diameter was around 230 nm (matched Figure S1). Besides, the elements distribution was tested by STEM. The EELS scan conducted with STEM imaging (Figure 2D,E) on a PLPs@$mSiO_2$ nanoparticle, indicating a higher concentration of Ca, Zn, Ti, and Pr elements in the central region of the nanoparticle, which was very matched with the expected core−shell structure.

Optical Performance of the (ICG+PLPs)@$mSiO_2$ Nanoparticles. The Optical performance of PLPs@$mSiO_2$ including excitation spectrum, emission spectrum, optical absorption spectrum, fluorescence imaging, and persistent luminescence imaging were tested by a UV−vis spectrophotometer, fluorescence spectrometer, and in vivo luminescence imaging system. With 314 nm ultraviolet light excitation, PLPs@$mSiO_2$ nanoparticles generated a pink emission band in about 600−650 nm and the emission maximum was at 625 nm (Figure 3A,B).

Furthermore, the PLPs@$mSiO_2$ nanoparticles showed very long persistent luminescence. The persistent luminescence intensity was detected at 625 nm after exposure for 5 min by 314 nm ultraviolet light and its luminescence reduced sharply in the first several minutes and then slowly decreased. After 2.5 h, the red long afterglow fluorescence still remained. This phenomenon indicated that PLPs@$mSiO_2$ nanoparticles could give a long-lasting persistent luminescence (Figure 3C).

The PLPs@$mSiO_2$ nanoparticles powders using as ink were printed on the hard paper to form an image of the "TJU" letters. These letters were illuminated for 5 min by ultraviolet light, and digital photo results showed bright luminescence (Figure 3D). Besides, the persistent luminescence of PLPs@$mSiO_2$ nanoparticles were also investigated by in vivo luminescence imaging system. The persistent luminescence imaging was measured within 40 min. There were six groups including the empty silica nanoparticles as control group and PLPs@$mSiO_2$ nanoparticles with different concentrations as experimental groups. Compared with the control group, the persistent luminescence signals of PLPs@$mSiO_2$ nanoparticles still existed even 40 min after removing ultraviolet lamp, showing that PLPs@$mSiO_2$ nanoparticles had excellent persistent luminescence property, which was consistent with the results mentioned above. At the same observation time point, with the increase of the concentration, the PLPs@$mSiO_2$ nanoparticles showed much brighter persistent luminescence (Figure 3G).

In order to confirm whether the ICG had been loaded into PLPs@$mSiO_2$ nanoparticles, the UV−vis optical absorption spectra and fluorescence emission spectra were measured. In the UV−vis optical absorption spectra, there were three

DOI: 10.1021/acsami.6b07642
ACS Appl. Mater. Interfaces 2016, 8, 21603−21611

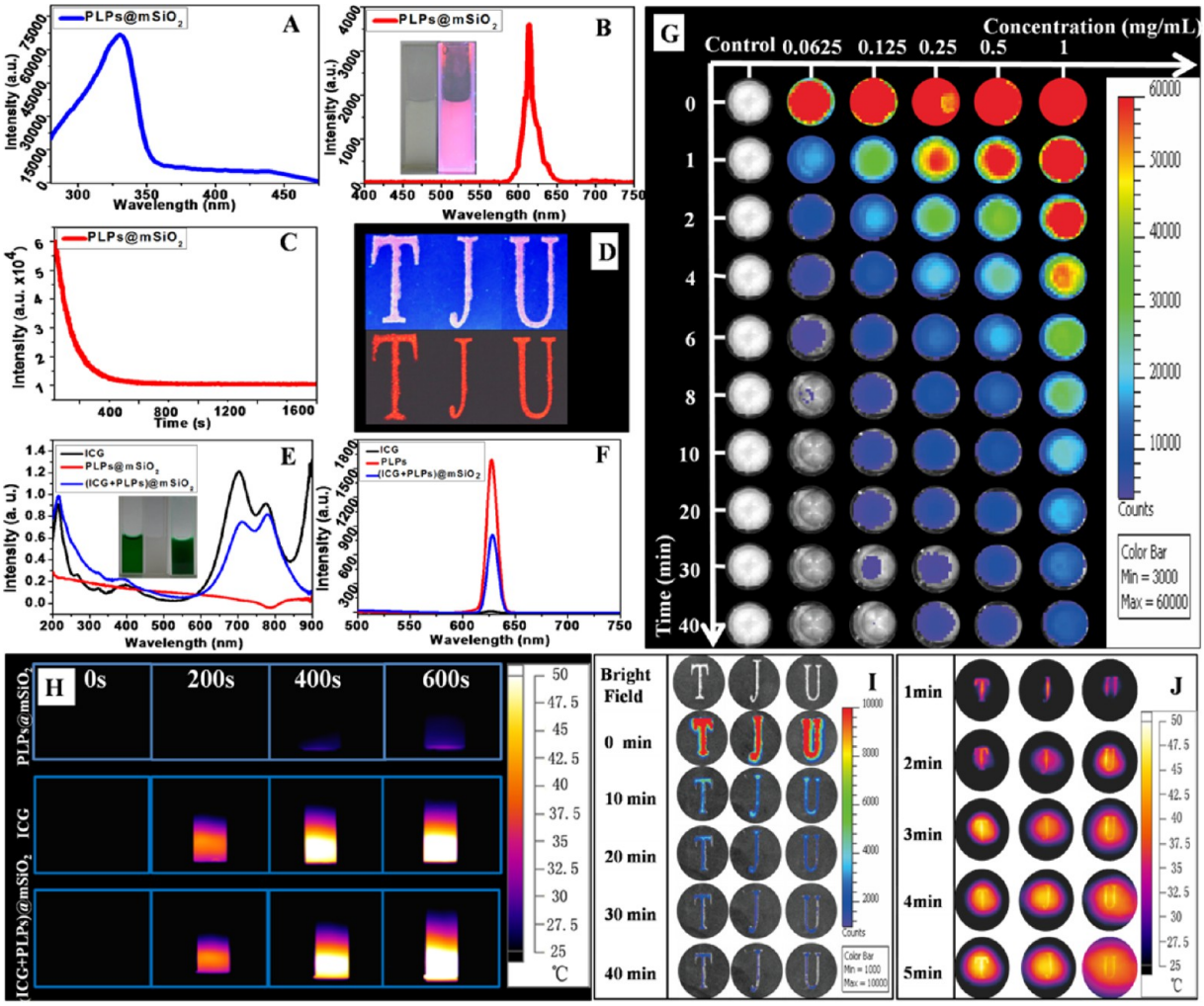

Figure 3. Optical and photothermal performance of the PLPs@mSiO$_2$ nanoparticles. (A) The excitation spectrum of PLPs@mSiO$_2$ nanoparticles. (B) The emission spectrum of PLPs@SiO$_2$ nanoparticles. The inserts showed the macrophotograph of the PLPs@mSiO$_2$ nanoparticles before and UV light exposure. (C) Long afterglow decay curve of PLPs@mSiO$_2$ nanoparticles. (D) The digital photo of the PLPs@mSiO$_2$ nanoparticles powered as ink were printed on the hard paper to form an image of the "TJU" letters under ultraviolet lamp irradiation and the lamp was removed after irradiating for 5 min. (E) The UV−vis absorption spectrum for ICG, PLPs@mSiO$_2$, and (ICG+PLPs)@mSiO$_2$. The inserts showed the macrophotograph of these samples. (F) The fluorescence spectrometer of ICG, PLPs@mSiO$_2$, and (ICG+PLPs)@mSiO$_2$ under UV light exposure. (G) The photothermal imaging of the persistent luminescence images of PLPs@mSiO$_2$ nanoparticles with different concentration was measured within 40 min. (H) The photothermal imagings of ICG, PLPs@mSiO$_2$, and (ICG+PLPs)@mSiO$_2$ within 10 min. (I) The persistent luminescence imagines of the (ICG+PLPs)@mSiO$_2$ nanoparticle powders as ink printed on the hard paper to form images of "TJU" letters within 40 min. (J) Photothermal imagings of the (ICG+PLPs)@mSiO$_2$ nanoparticle powders as ink printed on the hard paper to form images of "TJU" letters within 5 min.

samples including ICG, PLPs@mSiO$_2$ nanoparticles, and (ICG +PLPs)@mSiO$_2$ nanoparticles. The characteristic absorption peak of ICG was about 800 nm, which had deep tissue penetration during the photothermal therapy. After ICG was loaded into the PLPs@mSiO$_2$ nanoparticles, there was an emergence of a new absorption peak at about 800 nm for (ICG +PLPs)@mSiO$_2$ nanoparticles, which indicated that ICG had been successfully loaded into the PLPs@mSiO$_2$ nanoparticles (Figure 3E). Meanwhile, the fluorescence spectrometers of ICG, PLPs@mSiO$_2$, and (ICG+PLPs)@mSiO$_2$ were also detected. With 314 nm ultraviolet light excitation, the aqueous solution of (ICG+PLPs)@mSiO$_2$ nanoparticles generated a pink emission band in about 600−650 nm and the emission maximum was at 625 nm consistent with PLPs@mSiO$_2$ (Figure 3F).

Persistent Luminescence and Photothermal Performance of the (ICG+PLPs)@mSiO$_2$ Nanoparticles. It is generally known that the temperature in excess of 43 °C could damage tumor cells on account of their poor heat tolerance,[30] so photothermal effects were tested by exposing the samples to 808 nm near-infrared laser light and measuring temperature changes within 10 min. There were three samples including ICG, PLPs@mSiO$_2$ nanoparticles, and (ICG+PLPs) @mSiO$_2$ nanoparticles. The temperature increase in ICG solution was clearly observed within 10 min. ICG was loaded into PLPs@mSiO$_2$ nanoparticles to form the (ICG+PLPs)@ mSiO$_2$ nanoparticles, which could effectively absorb 808 nm near-infrared light to produce optothermal by the ICG. The maximum temperature of (ICG+PLPs)@mSiO$_2$ fleetly increased from 20 to 62 °C within 10 min under the 808 nm light irradiation, which exceeded the free ICG, 56 °C (Figure 3H

DOI: 10.1021/acsami.6b07642
ACS Appl. Mater. Interfaces 2016, 8, 21603−21611

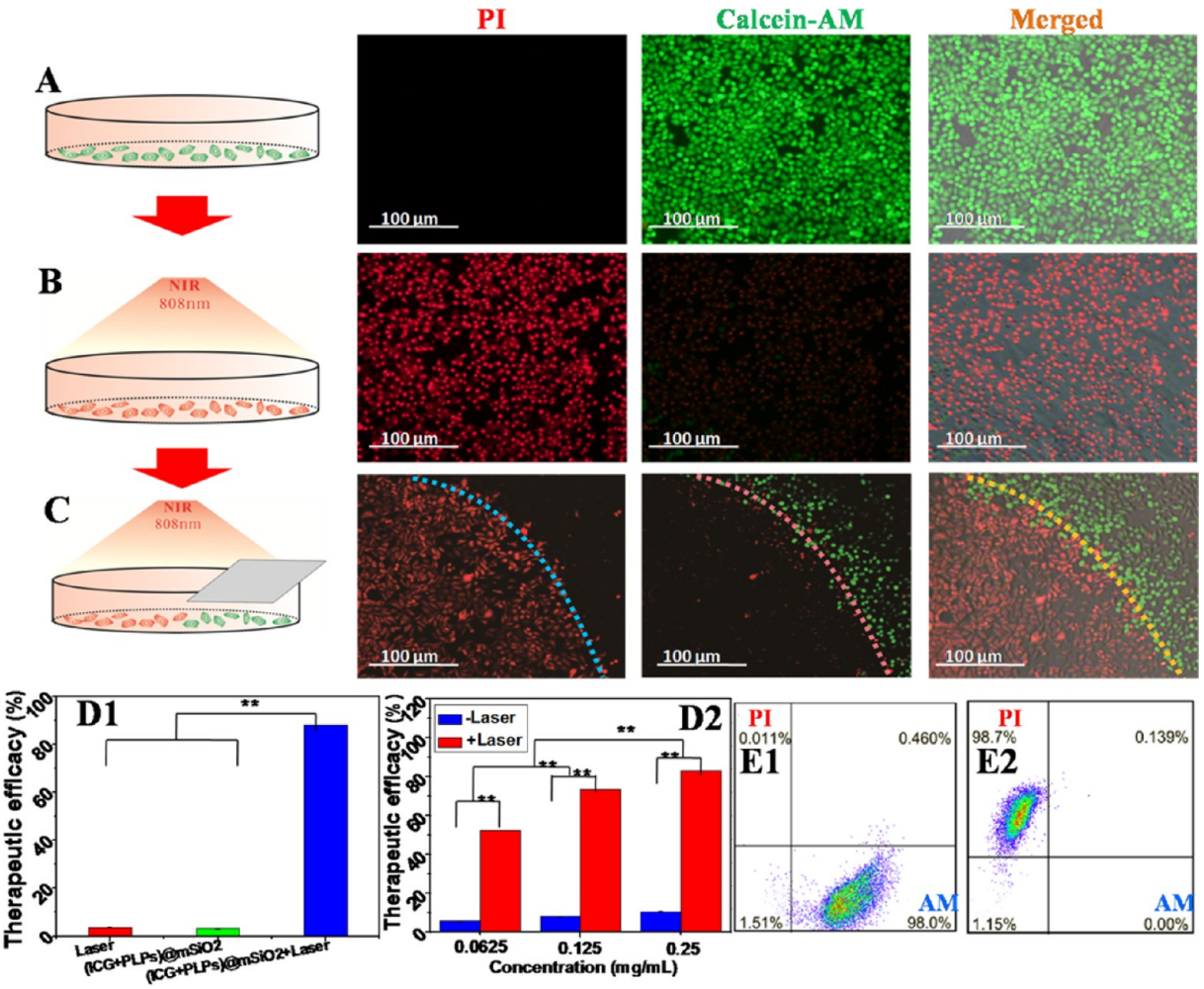

Figure 4. 808 nm near-infrared light selectively triggered PTT in cells by (ICG+PLPs)@mSiO$_2$ nanoparticles. Calcein-AM and PI were used for labeling living and death cells, respectively. (A) (ICG+PLPs)@mSiO$_2$ nanoparticles without near-infrared laser irradiation (Group 1). (B) (ICG +PLPs)@mSiO$_2$ nanoparticles with entire near-infrared laser irradiation (Group 2). (C) (ICG+PLPs)@mSiO$_2$ nanoparticles with sectional near-infrared laser irradiation (Group 3). (D1) PTT efficiency of different samples, including only 808 nm laser irradiation, (ICG+PLPs)@mSiO$_2$ nanoparticles without 808 nm laser irradiation, and (ICG+PLPs)@mSiO$_2$ nanoparticles with 808 nm laser irradiation, were quantified by MTT essay (n = 5). (D2) PTT efficiency of different concentration for (ICG+PLPs)@mSiO$_2$ nanoparticles was quantified by MTT essay (n = 5). (E1) PTT efficiency of part A was quantified with flow cytometry. (E2) PTT efficiency of part B was quantified with flow cytometry. The scale bars were 100 μm.

and Figure S7). This phenomenon also proved that the ICG loading process was successful, and the photothermal performance of (ICG+PLPs)@mSiO$_2$ nanoparticles was better than free ICG.

In order to test whether the same (ICG+PLPs)@mSiO$_2$ nanoparticles sample had both long persistent luminescence and photothermal performance, the (ICG+PLPs)@mSiO$_2$ nanoparticles powders using as ink were printed on the hard paper to form images of "TJU" letters. The long persistent luminescence and photothermal performance were, respectively, tested by an in vivo luminescence imaging system and thermal radiometer. As seen in Figure 3I, long persistent luminescence on the "TJU" letters could last for more than 40 min. Besides, the temperature increase on the same "TJU" letters was clearly observed within 5 min (Figure 3J). All of the results proved that the (ICG+PLPs)@mSiO$_2$ nanoparticles had both the performance of the light and heat at the same time, and it could be used as an agent for optical imaging-guided therapy.

Cytotoxicity Study and Cell Uptake Study of These Nanoparticles. The biocompatibility of these nanoparticles was tested by MTT assay, fluorescence imaging, and flow cytometry. As seen in Figure S8B, both of the ICG and (ICG +PLPs)@mSiO$_2$ nanoparticles did not cause obvious cytotoxicity when the concentration was lower than 1 mg/mL, suggesting that ICG and (ICG+PLPs)@mSiO$_2$ had good biocompatibility. After ICG was assembled into pores of mesoporous silica, cell viability still nearly kept the same, which indicated that PLPs@mSiO$_2$ had nearly no influence on the cell viability. When the concentration increased, the cell survival rate began to reduce in all these samples, but cell viability was still very high even at 1 mg/mL above 70% (Figure S8B). There were two groups, ICG solution as the control group and (ICG +PLPs)@mSiO$_2$ nanoparticles as the experimental group. The Calcein-AM as green fluorescent dye and propidium iodide (PI) as red fluorescent dye were used to label living cells and death cells, respectively. At 0.25 mg/mL of these two samples, nearly all the cells showed green fluorescence emitted from calcein-AM, suggesting that the cells were alive (Figure S8A).

DOI: 10.1021/acsami.6b07642
ACS Appl. Mater. Interfaces 2016, 8, 21603−21611

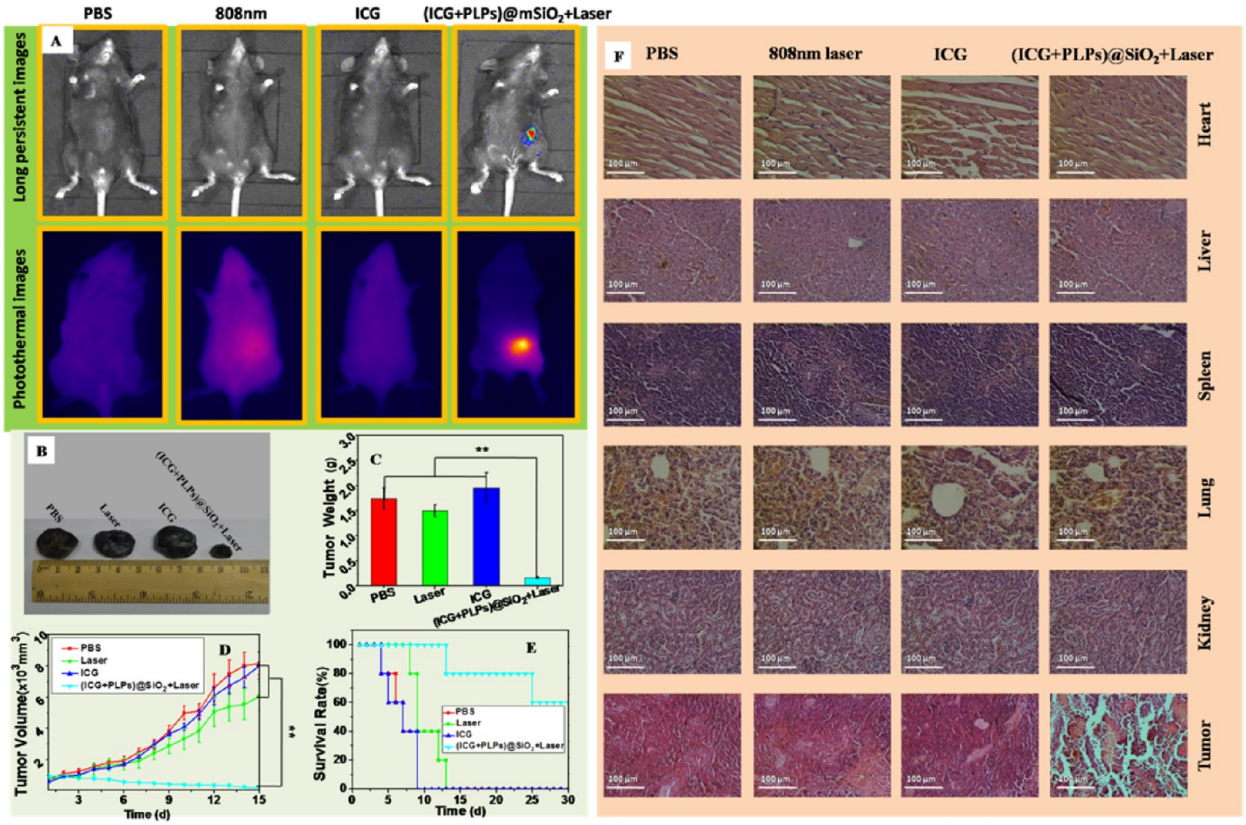

Figure 5. In vivo imaging and photothermal efficiency for tumor in mouse. (A) Imaging and photothermal property in vivo for PBS, 808 nm laser, free ICG none 808 nm laser, (ICG+PLPs)@$mSiO_2$ nanoparticles with 808 nm laser in the same mouse. (B) Size of melanoma tumors for treating with different samples after 15 days. (C) Change in melanoma tumor weight for treating with different samples after 15 days (n = 5). (D) Change in tumor volumes for treating with different samples within 30 days (n = 5). (E) Survival curve of B16 subcutaneous tumor model in C57/BL6 for treating with different samples (n = 5). (F) Hematoxylin and eosinsurvival stained for the major organs of mice and tumor after treating with different samples 15 days. (**) P < 0.01. The scale bars were 100 μm.

Besides, the same phenomenon was also observed by flow cytometry, and fluorescence scattergram results showed that the cells incubated with ICG or (ICG+PLPs)@$mSiO_2$ had strong green fluorescence, indicating that the cells were alive (Figure S8C).

The uptake of the ICG and (ICG+PLPs)@$mSiO_2$ by Hela cells were visualized by a confocal microscope (Figure S9). The blue fluorescence showed the DAPI labeled nucleus and the red fluorescence showed the ICG in cells. As shown in Figure S9, little ICG endocytosis was found in the free ICG group, and after 4 h incubation, more ICG was uptaken in (ICG+PLPs)@$mSiO_2$ nanoparticle group as evident from fluorescence microscopy, indicating that nanoparticle could improve cell endocytosis efficiency of ICG.

Photothermal Therapy Effect of (ICG+PLPs)@$mSiO_2$ Nanoparticles in Cancer Cells. To detect near-infrared light trigger-controlled PTT in living cells to (ICG+PLPs)@$mSiO_2$, they were cultivated with Hela cells. Then Calcein-AM and PI were used for labeling living and death cells, respectively. There were three groups including groups without near-infrared laser (Group 1), with the entire near-infrared laser (Group 2), and with sectional near-infrared laser (Group 3). As seen in Figure 4B, compared with Group1 (Figure 4A), in group 2 nearly all the cells showed red fluorescence emitted from PI, suggesting that the cells were dead after near-infrared laser exposure for 5 min, in Figure 4B. Besides, the same phenomenon was also confirmed by MTT assay (Figure 4D) and flow cytometry studies (Figure 4E). Meanwhile, to prove if the project could selectivity induce cells death at high resolution, (ICG+PLPs)@$mSiO_2$ nanoparticles were incubated with Hela cells. Instead of exposing the whole cell culture well, half of the hole was obstructed with foil and the remaining half was exposed to near-infrared light, see Figure 4C. Fluorescence microscope was used to check the cells death situation in Group 3. In Figure 4C, there was a stronger green fluorescencing cells in the covered area, while for the uncovered area, there appeared stronger red fluorescence. All these results showed that the (ICG+PLPs)@$mSiO_2$ nanoparticles could selectively control PTT in cells under NIR light accurate irradiation. Hence, our work turned into a novel technique for precisely regulating cell death by accurate NIR light irradiation.

Imaging and Photothermal Property of (ICG+PLPs)@$mSiO_2$ Nanoparticle in Vivo. For revealing theranostic and optothermal property in vivo, the (ICG+PLPs)@$mSiO_2$ was used in in vivo imaging and phototherapy. Due to the (ICG +PLPs)@$mSiO_2$ nanoparticles had stable long afterglow performance and strong penetrability in the organism, it could be well used for sostenuto in vivo imaging with no external excitation light source. Figure 5A and Figure S10 showed in vivo imaging of (ICG+PLPs)@$mSiO_2$ after subcutaneous injected into a living mouse. There was a strong afterglow emission signal after 20 min' observation for PLPs@$mSiO_2$ group and (ICG+PLPs)@$mSiO_2$ group (Figure 5A and Figure S10). Meanwhile, to prove the photothermal property of the (ICG+PLPs)@$mSiO_2$ nanoparticles in the same mice, the C57/BL6 mouse strain was selected and carried in a local

DOI: 10.1021/acsami.6b07642
ACS Appl. Mater. Interfaces 2016, 8, 21603−21611

injection experiment. The temperature changes were monitored under 808 nm laser exposure for realizing PTT. As shown in Figure 5A, the temperature rise of these groups were completely different after NIR irradiation of the persistent luminescence region for 5 min, compared with the PBS, only 808 irradiation, and ICG groups. It might be indicated that there were terrific light−heat properties for the same (ICG +PLPs)@$mSiO_2$ nanoparticles in vivo.

Additionally, the maximum temperature of (ICG+PLPs)@$mSiO_2$ quickly increased to 50 °C within 5 min under NIR exposure, compared with PLPs@$mSiO_2$ with 808 nm light irradiation (Figure S11). This phenomenon indicated that the (ICG+PLPs)@$mSiO_2$ was enough to destroy cancer cells. It would be that 808 nm light was effectively transformed into heat in vivo by (ICG+PLPs)@$mSiO_2$ and could be used to implement heat treatment as hyperthermia agents. The imaging results indicated that in view of the as-prepared (ICG+PLPs)@$mSiO_2$ nanoparticles without background luminescence or autofluorescence, the long persistence signal could be used to determine the location of the tumor for photothermal therapy and did not require additional excitation light.

In Vivo Photothermal Efficiency of Tumor in Mice. The PTT effect was further assessed in vivo with B16 subcutaneous tumor model in C57/BL6 mouse. Here, the group 1 only accepted PBS intratumoral injection, group 2 only received NIR irradiation, group 3 received ICG intratumoral injected only, and group 4 received the (ICG+PLPs)@$mSiO_2$ intratumoral injection and was irradiated with the NIR laser. As seen in Figure 5B, group 2 did not show obvious antitumor effect compared to group 1, indicating that 808 nm near-infrared light itself could not lead to an apparent destruction after irradiating for 5 min at 2.5 W/cm^2. On the contrary, the group mice of injection (ICG+PLPs)@$mSiO_2$ and then irradiation with the NIR laser showed very low tumor growth (Figure S12). These data showed that tumor growth was suppressed very well by (ICG+PLPs)@$mSiO_2$ with the 808 nm laser. Besides, each group of tumors in vitro photos were presented and displayed, and the tumor size of the group with injection (ICG+PLPs)@$mSiO_2$ and then irradiation with the NIR laser was a minimum, indicating that the (ICG+PLPs)@$mSiO_2$ group could effectively inhibit the growth of tumor, comparing to other groups such as PBS, 808 nm laser, and ICG (Figure 5B). Meanwhile, tumor size and weight changes showed that only the 808 nm near-infrared laser irradiation group could not significantly inhibit the growth of tumor (Figure 5C,D) compared with group 1, which also showed that the effect of thermal damage could be ignored by 808 nm near-infrared light. However, the group of injection (ICG+PLPs)@$mSiO_2$ and then irradiating with the NIR laser showed smaller tumor volumes and weight. The results indicated that when treated with (ICG+PLPs)@$mSiO_2$, tumors would probably acquire adequate temperature to cause destruction, while group 1 and group 3 would be insufficient to achieve tumor destruction ($P < 0.01$). What's more, the significant survival time was recorded for each group. It turned out that the group of injection (ICG+PLPs)@$mSiO_2$ and then irradiating with the NIR laser had a longer survival time than others (Figure 5E) ($P < 0.01$).

In addition, the B16 xenograft tumors were collected and stained with hematoxylin and eosin. In PBS injected only, 808 laser irradiation only, and ICG injected only groups, poorly differentiated histology and the dense fibrotic tissue were discovered, and no vasculature could be observed inside tumor cell nests (Figure 5F), which was corresponded to the characteristics of the B16 xenograft tumor tissue described in earlier references. However, the tumor cells in (ICG+PLPs)@$mSiO_2$ under the 808 nm laser group exhibited obvious structural destruction and necrosis. In the meantime, the major organs of mice treated were collected for histological staining to compare with the control groups. No appreciable abnormality was observed in heart, liver, spleen, lung, and kidneys (Figure 5F). In the process of all animal experiments, the weight of rats were recorded and results showed that all groups weight of mice with a tumor had no obvious change (Figure S13). The results indicated that photothermal therapy of (ICG+PLPs)@$mSiO_2$ with 808 nm laser treatment could be tolerant and had no apparent toxic and side effects in vivo. In brief, these facts illustrated the combination of the overheating effect derived from (ICG+PLPs)@$mSiO_2$ mediated PTT and obtained a desirable phototherapy outcome for effective remission of tumors growth in vivo.

CONCLUSION

In conclusion, we have successfully fabricated Indocyanine green (ICG) and persistent luminescence phosphors coloaded mesoporous silica nanoparticles ((ICG+PLPs)@$mSiO_2$) for persistent luminescent imaging-guided photothermal therapy (PTT). The in vivo imaging and thermal effects of red broad afterglow and ICG were perfectly integrated into the system among PLPs tracker photothermal therapy by high signal-to-noise ratio in vivo for minimized adverse effect by accurate visual treatment. In this study, the system exhibited excellent fluorescence stability and enhanced temperature response. On the basis of these excellent properties, the new kind of (ICG +PLPs)@$mSiO_2$ nanoparticles could improve the signal-to-noise ratio during luminescence imaging-guided PTT, and the irradiation to tumor could be selectively and efficiently controlled by a NIR-trigger. Besides, histological results indicated no obvious toxicity of (ICG+PLPs)@$mSiO_2$ to the laboratory animal. Hence, this kind of new long afterglow nanoparticles had great potential for various tumors accurate treatment as a tracker, such as phosphorescent markers, nanoprobed, drug carriers, and so on.

MATERIALS AND METHODS

Materials. Indocyanine green (ICG, United States Pharmacopeia (USP) Reference Standard), calcium nitrate tetrahydrate ($Ca(NO_3)_2 \cdot 4H_2O$, ≥99.0%), zinc nitrate ($Zn(NO_3)_2 \cdot 4H_2O$, ≥99.0%), praseodymium nitrate hexahydrate ($Pr(NO_3)_3 \cdot 6H_2O$, ≥99.9%), titanium(IV) butoxide ($Ti(OC_4H_9)_4$, 97%), and nitric acid were obtained from Sigma-Aldrich; tetraethylorthosilicate (TEOS, ≥99%), cetyltrimethylammonium bromide (CTAB, ≥99%), sodium chloride (NaCl, ≥99.0%), sodium hydroxide (NaOH, ≥98%) were obtained from Sigma-Aldrich. Water was purified according to refs 31 and 32.

Synthesis of $CaZnTiO_3$:0.1% Pr^{3+} Persistent Luminescent Phosphors (PLPs). $CaZnTiO_3$:0.1% Pr^{3+} persistent luminescent phosphors was synthesized by the sol−gel method.[33] Generally, $Ca(NO_3)_2 \cdot 4H_2O$, $Zn(NO_3)_2 \cdot 4H_2O$, $Pr(NO_3)_3 \cdot 6H_2O$, and $Ti(OC_4H_9)_4$ were used as the starting materials. First, $Ti(OC_4H_9)_4$ and nitric acid were used to synthesize titanyl nitrate. Next, $Pr(NO_3)_3 \cdot 6H_2O$ and $Ca(NO_3)_2 \cdot 4H_2O$ were added to the titanyl nitrate solution. The mixed solution was put in 70 °C for stirring for 2 h. Then, the white precursor was collected and heated in a sintering furnace at 1100 °C, 3 h. Finally, $CaZnTiO_3$:0.1% Pr^{3+} persistent luminescent phosphors were ground by a ball grinder and purified by centrifugation.

Synthesis of $CaZnTiO_3$:0.1% Pr^{3+} Persistent Luminescent Phosphors Loaded Mesoporous Silica Nanoparticles (PLPs@$mSiO_2$), ICG, and PLPs Coloaded $mSiO_2$ Nanoparticles (ICG

DOI: 10.1021/acsami.6b07642
ACS Appl. Mater. Interfaces 2016, 8, 21603−21611

+PLPs)@mSiO$_2$. PLPs@mSiO$_2$ nanoparticles were synthesized by the CTAB template method.[31,32] ICG and PLPs@mSiO$_2$ coloaded (ICG +PLPs)@mSiO$_2$ nanoparticles were synthesized according to the following method. Briefly, ICG powder (5−20 mg) was dissolved into PLPs@mSiO$_2$ aqueous solution (10 mL) and stirred. Finally, the nanoparticles were characterized and the cytotoxicity assays of them were performed, according to refs 31 and 32.

Persistent Luminescent Imaging, Photothermal Efficiency and Photothermal Therapy Efficiency of Different Samples in Vitro and in Vivo. In vitro persistent luminescent phosphors were put into a 96-well plate for imaging by an in vivo imaging instrument. The luminescent intensity from nanoparticles were monitored after UV light irradiation for 5 min. The in vivo imaging of mice was detected after injection of the nanoparticles dissolving in PBS through the subcutaneous. To test photothermal therapy efficiency, various samples were added into quartz cell. Using a 2.5 W/cm^2 808 nm NIR laser to irradiate these samples for 10 min simultaneously, and each group of temperature changes was monitored using a thermal imaging camera. To explore the PTT efficacy, different samples were incubated with cells for 24 h and then washed by PBS. The cell viability was detected after the laser irradiation destination region with the MTT assay mentioned above. Cytotoxicity of PTT was also detected using Calcein-AM/PI dying. Besides, the cells were dyed with Calcein-AM for living cell and propidium iodide for death cell visualization following the manufacturer's suggestion (Invitrogen).

To prove the photothermal therapy efficiency of different samples in vivo, female C57/B6 mice (8 weeks) purchased from Beijing HFK Bioscience Co., Ltd. The melanoma tumor model was performed by injecting 5 × 10^5 B16 cells for 1 week. The tumor volume and weight were calculated according to ref 34. In addition, the histological analysis and statistical analysis were performed according to ref 34.

■ ASSOCIATED CONTENT

Supporting Information

The Supporting Information is available free of charge on the ACS Publications website at DOI: 10.1021/acsami.6b07642.

Particle size of mSiO$_2$, PLPs@mSiO$_2$, (ICG+ PLPs) @ mSiO$_2$; emission spectra of PLPs and ultraviolet absorption spectrum of ICG; UV−vis spectra and standard cure of ICG; fluorescence spectra of ICG, PLPs@mSiO$_2$, and (ICG+PLPs) @mSiO$_2$; temperature rise curves for different concentration, power, and sample for ICG, PLPs@mSiO$_2$, and (ICG+PLPs)@mSiO$_2$ under 808 nm laser; cytotoxicity study; cell uptake study of free ICG and (ICG+PLPs)@mSiO$_2$; persistent luminescence property of PLPs@mSiO$_2$ and (ICG+PLPs)@mSiO$_2$ in vivo; photothermal property of PLPs@mSiO$_2$ and (ICG +PLPs)@mSiO$_2$ in vivo; in vivo photothermal efficiency of tumor growth and weight change of mice for treating with PBS, only 808 irradiation, ICG without 808 irradiation, and (ICG+PLPs)@mSiO$_2$ under 808 irradiation (PDF)

■ AUTHOR INFORMATION

Corresponding Authors

*E-mail: wanghj@tju.edu.cn.

*E-mail: jinchang@tju.edu.cn.

Author Contributions

#Dr. Zheng and Dr. Chen contributed equally to this work.

Notes

The authors declare no competing financial interest.

■ ACKNOWLEDGMENTS

The authors gratefully acknowledge National Natural Science Foundation of China (Grants 51373117, 51303126, 51573128, and 81402575) and Tianjin Natural Science Foundation (Grants 13JCZDJC33200 and 15JCQNJC03100).

■ REFERENCES

(1) Ju, E.; Dong, K.; Liu, Z.; Ren, J.; Qu, X. Tumor Microenvironment Activated Photothermal Strategy for Precisely Controlled Ablation of Solid Tumors upon NIR Irradiation. *Adv. Funct. Mater.* **2015**, *25* (10), 1574−1580.

(2) Wang, Z.; Chen, Z.; Liu, Z.; Shi, P.; Dong, K.; Ju, E.; Ren, J.; Qu, X. A Multi-Stimuli Responsive Gold Nanocage−Hyaluronic Platform for Targeted Photothermal and Chemotherapy. *Biomaterials* **2014**, *35* (36), 9678−88.

(3) Dong, K.; Liu, Z.; Li, Z.; Ren, J.; Qu, X. Hydrophobic Anticancer Drug Delivery by a 980 nm Laser-Driven Photothermal Vehicle for Efficient Synergistic Therapy of Cancer Cells In Vivo. *Adv. Mater.* **2013**, *25* (32), 4452−4458.

(4) Jaque, D.; Martinez Maestro, L.; del Rosal, B.; Haro-Gonzalez, P.; Benayas, A.; Plaza, J. L.; Martin Rodriguez, E.; Garcia Sole, J. Nanoparticles for Photothermal Therapies. *Nanoscale* **2014**, *6* (16), 9494−9530.

(5) Austin, L. A.; Mackey, M. A.; Dreaden, E. C.; El-Sayed, M. A. The Optical, Photothermal, and Facile Surface Chemical Properties of Gold and Silver Nanoparticles in Biodiagnostics, Therapy, and Drug Delivery. *Arch. Toxicol.* **2014**, *88* (7), 1391−1417.

(6) Yuan, A.; Wu, J.; Tang, X.; Zhao, L.; Xu, F.; Hu, Y. Application of Near-Infrared Dyes for Tumor Imaging, Photothermal, and Photodynamic Therapies. *J. Pharm. Sci.* **2013**, *102* (1), 6−28.

(7) Zheng, M.; Zhao, P.; Luo, Z.; Gong, P.; Zheng, C.; Zhang, P.; Yue, C.; Gao, D.; Ma, Y.; Cai, L. Robust ICG Theranostic Nanoparticles for Folate Targeted Cancer Imaging and Highly Effective Photothermal Therapy. *ACS Appl. Mater. Interfaces* **2014**, *6* (9), 6709−6716.

(8) Zheng, M.; Yue, C.; Ma, Y.; Gong, P.; Zhao, P.; Zheng, C.; Sheng, Z.; Zhang, P.; Wang, Z.; Cai, L. Single-Step Assembly of DOX/ICG Loaded Lipid-Polymer Nanoparticles for Highly Effective Chemo-photothermal Combination Therapy. *ACS Nano* **2013**, *7* (3), 2056−2067.

(9) Ocsoy, I.; Isiklan, N.; Cansiz, S.; Ozdemir, N.; Tan, W. ICG-Conjugated Magnetic Graphene Oxide for Dual Photothermal and Photodynamic Therapy. *RSC Adv.* **2016**, *6* (36), 30285−30292.

(10) Desmettre, T.; Devoisselle, J. M.; Mordon, S. Fluorescence Properties and Metabolic Features of Indocyanine Green (ICG) as Related to Angiography. *Surv. Ophthalmol.* **2000**, *45* (1), 15−27.

(11) Yu, J.; Javier, D.; Yaseen, M. A.; Nitin, N.; Richards-Kortum, R.; Anvari, B.; Wong, M. S. Self-Assembly Synthesis, Tumor Cell Targeting, and Photothermal Capabilities of Antibody-Coated Indocyanine Green Nanocapsules. *J. Am. Chem. Soc.* **2010**, *132* (6), 1929−1938.

(12) Kuo, W.-S.; Chang, Y.-T.; Cho, K.-C.; Chiu, K.-C.; Lien, C.-H.; Yeh, C.-S.; Chen, S.-J. Gold Nanomaterials Conjugated with Indocyanine Green for Dual-Modality Photodynamic and Photothermal Therapy. *Biomaterials* **2012**, *33* (11), 3270−3278.

(13) Abels, C.; Fickweiler, S.; Weiderer, P.; Baumler, W.; Hofstadter, F.; Landthaler, M.; Szeimies, R. M. Indocyanine Green (ICG) and Laser Irradiation Induce Photooxidation. *Arch. Dermatol. Res.* **2000**, *292* (8), 404−411.

(14) Zheng, X.; Xing, D.; Zhou, F.; Wu, B.; Chen, W. R. Indocyanine Green-Containing Nanostructure as Near Infrared Dual-Functional Targeting Probes for Optical Imaging and Photothermal Therapy. *Mol. Pharmaceutics* **2011**, *8* (2), 447−456.

(15) Ma, Y.; Tong, S.; Bao, G.; Gao, C.; Dai, Z. Indocyanine Green Loaded SPIO Nanoparticles with Phospholipid-PEG Coating for Dual-Modal Imaging and Photothermal Therapy. *Biomaterials* **2013**, *34* (31), 7706−7714.

(16) Sharma, P.; Brown, S.; Walter, G.; Santra, S.; Moudgil, B. Nanoparticles for Bioimaging. *Adv. Colloid Interface Sci.* **2006**, *123-126*, 471−485.

(17) Lee, J. E.; Lee, N.; Kim, H.; Kim, J.; Choi, S. H.; Kim, J. H.; Kim, T.; Song, I. C.; Park, S. P.; Moon, W. K.; Hyeon, T. Uniform

Mesoporous Dye-Doped Silica Nanoparticles Decorated with Multiple Magnetite Nanocrystals for Simultaneous Enhanced Magnetic Resonance Imaging, Fluorescence Imaging, and Drug Delivery. *J. Am. Chem. Soc.* **2010**, *132* (2), 552−557.
(18) Michalet, X.; Pinaud, F. F.; Bentolila, L. A.; Tsay, J. M.; Doose, S.; Li, J. J.; Sundaresan, G.; Wu, A. M.; Gambhir, S. S.; Weiss, S. Quantum Dots for Live Cells, in Vivo Imaging, and Diagnostics. *Science* **2005**, *307* (5709), 538−544.
(19) Abdukayum, A.; Chen, J. T.; Zhao, Q.; Yan, X. P. Functional Near Infrared-Emitting Cr^{3+}/Pr^{3+} Co-Doped Zinc Gallogermanate Persistent Luminescent Nanoparticles with Superlong Afterglow for in Vivo Targeted Bioimaging. *J. Am. Chem. Soc.* **2013**, *135* (38), 14125−14133.
(20) De Chermont, Q. L. M.; Chanéac, C.; Seguin, J.; Pellé, F.; Maîtrejean, S.; Jolivet, J. P.; Scherman, D. Nanoprobes with Near-Infrared Persistent Luminescence for in Vivo Imaging. *Proc. Natl. Acad. Sci. U. S. A.* **2007**, *104* (22), 9266−9271.
(21) Zhuang, Y.; Katayama, Y.; Ueda, J.; Tanabe, S. A Brief Review on Red to Near-Infrared Persistent Luminescence in Transition-Metal-Activated Phosphors. *Opt. Mater.* **2014**, *36* (11), 1907−1912.
(22) Clabau, F.; Rocquefelte, X.; Jobic, S.; Deniard, P.; Whangbo, M. H.; Garcia, A.; Le Mercier, T. Mechanism of Phosphorescence Appropriate for the Long-Lasting Phosphors Eu^{2+}-Doped $SrAl_2O_4$ with Codopants Dy^{3+} and B^{3+}. *Chem. Mater.* **2005**, *17* (15), 3904−3912.
(23) Van den Eeckhout, K.; Smet, P. F.; Poelman, D. Persistent Luminescence in Eu^{2+}-Doped Compounds: A Review. *Materials* **2010**, *3* (4), 2536−2566.
(24) Maldiney, T.; Bessiere, A.; Seguin, J.; Teston, E.; Sharma, S. K.; Viana, B.; Bos, A. J. J.; Dorenbos, P.; Bessodes, M.; Gourier, D.; Scherman, D.; Richard, C. The in Vivo Activation of Persistent Nanophosphors for Optical Imaging of Vascularization, Tumours and Grafted cells. *Nat. Mater.* **2014**, *13* (4), 418−426.
(25) Li, Z.; Zhang, Y.; Wu, X.; Huang, L.; Li, D.; Fan, W.; Han, G. Direct Aqueous-Phase Synthesis of Sub-10 nm "Luminous Pearls" with Enhanced in Vivo Renewable Near-Infrared Persistent Luminescence. *J. Am. Chem. Soc.* **2015**, *137* (16), 5304−5307.
(26) Maldiney, T.; Remond, M.; Bessodes, M.; Scherman, D.; Richard, C. Controlling Aminosilane Layer Thickness to Extend the Plasma Half-Life of Stealth Persistent Luminescence Nanoparticles in Vivo. *J. Mater. Chem. B* **2015**, *3* (19), 4009−4016.
(27) Sun, M.; Li, Z. J.; Liu, C. L.; Fu, H. X.; Shen, J. S.; Zhang, H. W. Persistent Luminescent Nanoparticles for Super-Long Time in Vivo and in Situ Imaging with Repeatable Excitation. *J. Lumin.* **2014**, *145*, 838−842.
(28) Wu, B. Y.; Wang, H. F.; Chen, J. T.; Yan, X. P. Fluorescence Resonance Energy Transfer Inhibition Assay for α-Fetoprotein Excreted During Cancer Cell Growth Using Functionalized Persistent Luminescence Nanoparticles. *J. Am. Chem. Soc.* **2011**, *133* (4), 686−688.
(29) Yin, S.; Chen, D.; Tang, W. Combustion Synthesis and Luminescent Properties of $CaTiO_3$: Pr, Al Persistent Phosphors. *J. Alloys Compd.* **2007**, *441* (1−2), 327−331.
(30) Shibu, E. S.; Hamada, M.; Murase, N.; Biju, V. Nanomaterials Formulations for Photothermal and Photodynamic Therapy of Cancer. *J. Photochem. Photobiol., C* **2013**, *15*, 53−72.
(31) Zheng, B.; Su, L.; Pan, H.; Hou, B.; Zhang, Y.; Zhou, F.; Chang, J. NIR-Remote Selected Activation Gene Expression in Living Cells by Upconverting Microrods. *Adv. Mater.* **2016**, *28*, 707−714.
(32) Zheng, B.; Gong, X.; Wang, S.; Wang, H.; Chang, J. A NIR-remote Controlled Recyclable Upconverting Nanoparticle: An Improved Tool for Live Cell Dye-Labeling. *Nanomedicine* **2016**, *12* (2), 472−473.
(33) Li, Z.-J.; Zhang, Y.-J.; Zhang, H.-W.; Fu, H.-X. Long-lasting Phosphorescence Functionalization of Mesoporous Silica Nanospheres by $CaTiO_3$:Pr^{3+} for Drug Delivery. *Microporous Mesoporous Mater.* **2013**, *176*, 48−54.
(34) Yan, F.; Wu, H.; Liu, H.; Deng, Z.; Liu, H.; Duan, W.; Zheng, H. Molecular Imaging-Guided Photothermal/Photodynamic Therapy Against Tumor by Irgd-Modified Indocyanine Green Nanoparticles. *J. Controlled Release* **2016**, *224*, 217−228.

DOI: 10.1021/acsami.6b07642
ACS Appl. Mater. Interfaces 2016, 8, 21603−21611